ASIAN JOURNAL OF PHARMACEUTICAL AND CLINICAL RESEARCH

INNOVARE ACADEMIC SCIENCES
Knowledge to Innovation

Vol 18, Issue 6, 2025

Online - 2455-3891
Print - 0974-2441

Research Article

IMPACT OF SUBSTITUENTS IN INDOLOBENZAZOCIN-8-ONE DERIVATIVES ON ANTICANCER ACTIVITY: INSIGHTS FROM MOLECULAR DOCKING AND ADMET PREDICTIONS

ARTHORN LOISRUANGSIN*, SASIWADEE BOONYA-UDTAYAN, WEENAWAN SOMPHON

Department of Physical and Material Sciences, Faculty of Liberal Arts and Science, Kasetsart University (Kamphaeng-Saen Campus), Nakhon Pathom, Thailand.
***Corresponding author: Arthorn Loisruangsin; Email: faasatl@ku.ac.th**

Received: 20 March 2025, Revised and Accepted: 05 May 2025

ABSTRACT

Objectives: The objective of the study is to explore how substitutions modulate indolobenzazocin-8-one's anticancer activity and advantages over taxanes using computational modeling.

Methods: Molecular docking predicted binding affinities (E_i, kcaL/moL) at β-tubulin's colchicine site, while ADMET models evaluated physicochemical/pharmacokinetic properties. Spearman's rank correlation analysis was employed for assessing structural- activity relationships.

Results: Cytotoxicity was primarily driven by cellular permeability, evidenced by a strong negative correlation between lipophilicity and potency ($logD_{7.4}$-IC_{50}: ρ=−0.90, p=0.037), unlike the weak, non-significant association with binding affinity (Ei-IC_{50}: ρ=0.46, p=0.434). Methoxy substitution weakened binding (ΔE_i increased up to 4.2 kcaL/moL) and had non-linear lipophilicity effects (mono-substitution: $\Delta logD_{7.4}$=+0.031; di-substitution: $\Delta logD_{7.4}$=−0.128). Hydroxy substitution enhanced affinity (ΔEi=−1.58 kcaL/moL) but compromised permeability ($\Delta logD_{7.4}$=−0.095). The optimized lead compound balanced these trade-offs, showing high intestinal absorption (Caco-2 permeability (log cm/s)=−5.033) and low P-glycoprotein efflux risk (probability=0.117).

Conclusion: Substitutions affect anticancer activity by altering both hydrophobicity and binding affinity. Unsubstituted indolobenzazocin-8-one demonstrated the most potent anticancer activity. In addition, its drug-like properties and bypass of P-gp-mediated resistance position it as a superior oral alternative to taxanes.

Keywords: Molecular docking, Pharmacokinetics, Indolobenzazocin-8-one, Tubulin polymerization.

 DOI: http://dx.doi.org/10.22159/ajpcr.2025v18i6.53858. Journal homepage: https://innovareacademics.in/journals/index.php/ajpcr

INTRODUCTION

Indolobenzazocin-8-one derivatives, which were synthesized using a palladium-catalyzed reaction and an internal amidation reaction of benzo[d]azocinones, were evaluated for their cytotoxic efficacy against cancer cell lines. Notably, the unsubstituted indolobenzazocin-8-one derivative showed superior activity among the synthesized compounds, with potent nanomolar-range cytotoxicity against both HepG2 and MOLT-3 cancer cell lines [1]. Although structure-activity relationships (SAR) were observed, the precise molecular mechanisms by which substituents modulate the anti-cancer activity of indolobenzazocin-8-one derivatives remain to be elucidated. Accumulating evidence indicates that indole derivatives exert anticancer effects through tubulin polymerization inhibition [2-7]. Indole-based compounds bind to tubulin at the colchicine-binding site [8-15]. While anti-cancer drug efficacy is multifactorial, their ability to penetrate cancer cells and selectively bind to molecular targets remains a fundamental requirement. Using computational modeling, we systematically analyzed how indolobenzazocin-8-one substituents affect these two factors, revealing critical structural determinants of anti-cancer activity. Furthermore, the pharmacokinetic properties of the top-performing derivative were analyzed to highlight its advantages over taxanes, a class of tubulin polymerization-inhibiting anticancer drugs.

MATERIALS AND METHODS

Materials

Docking calculations were conducted on a PC equipped with an Intel Core i5-12400 processor and 8 GB DDR4 RAM (1200 MHz), running Debian 12.0. The following software packages were employed: Avogadro [16] for molecular preparation, UCSF Chimera [17] for visualization, AutoDock4 and AutoDockTools4 [18] for docking simulations, and LigPlot+ [19] for interaction analysis, Microsoft Excel [20] for Spearman's rank correlation analysis. Physicochemical and pharmacokinetic properties of the indolobenzazocin-8-one derivatives were predicted using OpenBabel [21] and ADMETlab [22]. Two-dimensional molecular structures were generated with ChemSketch [23].

Methods

The indolobenzazocin-8-one derivatives were prepared through molecular modeling using Avogadro [16] with structures saved in protein data bank (PDB) format. Tubulin protein structures (PDB ID: 6NNG) were retrieved from the RCSB PDB; non-essential molecules were removed, and hydrogen atoms were added using UCSF Chimera [17].

To validate the docking protocol, redocking was performed by extracting the co-crystallized ligand (DJ95) from the tubulin structure and re-docking it into the original binding site using AutoDock4. The root-mean-square deviation (RMSD) between the redocked pose and the crystallographic pose was calculated to assess reproducibility, with an RMSD <2.0 Å considered acceptable [24].

Molecular dockings between the colchicine-binding site of tubulin and the derivatives were performed with AutoDock4 [18], and the optimal conformation along with binding affinity (E_i) was determined using AutoDockTools4 [18]. Ligand–protein interaction diagrams were generated as 2D plots using LigPlot+ [19]. Given the small sample size (n=5) and potential non-normal distribution of the data, non-parametric Spearman's rank correlation analysis was employed instead of Pearson's correlation. This approach is more robust for

assessing monotonic relationships without assumptions of normality or linearity [25].

For physicochemical and pharmacokinetic profiling, the derivatives' PDB structures were converted to SMILES format through Open Babel [21] and analyzed using ADMETlab [22]. Trends in E_i and permeability-related physicochemical properties were correlated with reported HepG2 cytotoxicity (IC_{50}) data from Boonya-Udtayan *et al*. [1]. Finally, the pharmacokinetic advantages of the most potent derivatives were benchmarked against taxane-based drugs using ADMETlab-derived parameters.

RESULTS AND DISCUSSION

Validation of molecular docking protocol

The tubulin structure was co-crystallized with DJ95 at the colchicine-binding site, which provided an ideal system to validate the accuracy of our molecular docking protocol through redocking. The calculated RMSD between the redocked DJ95 pose and its original crystallographic pose was 1.55 Å (Fig. 1), confirming that the docking protocol used in this study is reliable and acceptable.

Impact of substituent groups on the anticancer activity of indolobenzazocin-8-one derivatives

To investigate the SAR, derivatives with varying substituents at the R^1, R^2, R^3, and R^4 positions (Fig. 2) were systematically evaluated for their anticancer activity.

This SAR study initially examined unsubstituted indolobenzazocin-8-one derivatives as the baseline, followed by systematic evaluation of methoxy (-OCH_3) and hydroxy (-OH) substitutions. All analyzed structures were limited to those experimentally synthesized and characterized by Boonya-Udtayan *et al*. [1]. The two key parameters – tubulin binding affinity and cellular permeability – were quantified as follows: (i) Binding affinity (E_i) for tubulin interaction and (ii) octanol-water distribution coefficient at physiological pH ($logD_{7.4}$) [26] as permeability surrogate. These comparative data are presented in Table 1.

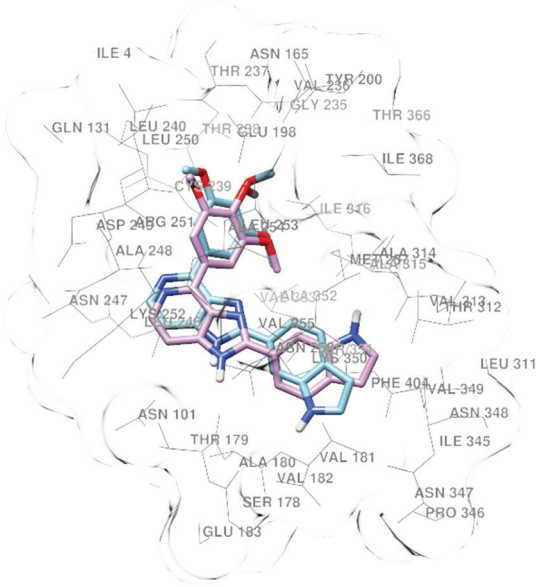

Fig. 1: Structural superpositions of redocked DJ95pose (pink) and its original crystallographic pose (blue) (root-mean-square deviation=1.55 Å) in the tubulin colchicine-binding site, generated using UCSF Chimera [17]

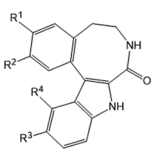

Fig. 2: Molecular structure of indolobenzazocin-8-one highlighting the variable substituent positions (R^1, R^2, R^3, and R^4)

Structure 1 (unsubstituted parent compound) demonstrated the most potent anticancer activity, exhibiting the lowest IC_{50} value (0.46 µM) against HepG2 cells. This enhanced cytotoxicity correlated with two key molecular characteristics: (i) The strongest binding affinity to tubulin, as evidenced by the lowest calculated binding affinity (E_i=−8.76 kcaL/moL) and (ii) superior membrane permeability potential, reflected by the highest experimental $logD_{7.4}$ value (2.263) among all derivatives. These results suggest that the unmodified scaffold achieves the optimal balance between target engagement and cellular uptake. The Structure 1's orientation in the binding pocket and the interacting amino acid residues are shown in Fig. 3a and Fig. 4a, respectively.

Structure 2, featuring –OCH_3 substitutions at both R^1 and R^2 positions of the benzazocine core, exhibited weaker tubulin binding affinity (E_i=−7.49 kcaL/moL) compared to the unsubstituted parent compound (Structure 1, E_i=−8.76 kcaL/moL). This 1.27 kcaL/moL reduction in binding energy was accompanied by a substantial conformational change in the binding mode, as evidenced by RMSD of 6.049 Å relative to structure 1 (Fig. 3b). The steric bulk of the methoxy substituents appears to enforce this alternative binding pose, which likely disrupts optimal protein-ligand interactions (Fig. 4b). Despite the intrinsic lipophilicity of methoxy groups, Structure 2 exhibited a reduced $logD_{7.4}$ value (2.135) compared to Structure 1 (2.263), suggesting decreased cellular permeability. This apparent paradox may be explained by (i) conformational changes induced by the -OCH_3 substitutions. Their steric effects likely force the molecule into a less planar configuration, thereby reducing overall membrane penetration potential [27]. This is consistent with the observed 6.049 Å RMSD shift in binding pose, which indicates significant structural reorganization. (ii) The electron-withdrawing nature of oxygen atoms of the dual methoxy substitutions at adjacent positions creates an asymmetric electron density distribution, inducing localized dipole moments. This electronic imbalance is exacerbated by the proximal positioning of two methoxy groups, which synergistically distort electron density toward their oxygen atoms through combined inductive effects. Concurrent deterioration in both binding energy (+1.27 kcaL/moL) and $logD_{7.4}$ (−0.128) aligned with Structure 2's impaired activity (IC_{50}=96.23 µM), highlighting the importance of balanced molecular properties for anticancer efficacy. While both attenuated binding affinity and compromised permeability likely contributed to the elevated IC_{50}, their individual weightings could not be definitively established from the current data.

Compared to Structure 2, the R^3 methoxy substitution of Structure 3 imposed two destabilizing effects: (i) Steric clash-induced pose deviation (1.537 Å RMSD from Structure 2; Fig. 3c) and (ii) elongation

Table 1: Structural features, HepG2 cytotoxicity (IC_{50}), tubulin binding affinity (E_i), and octanol-water partition coefficients ($logD_{7.4}$) of indolobenzazocin-8-one derivatives

Structure	Substituent groups	IC_{50}* (µM)	E_i (kcaL/moL)	log $D_{7.4}$
1	R^1=R^2=R^3=R^4=H	0.46	−8.76	2.263
2	R^1=R^2=OCH_3; R^3=R^4=H	96.23	−7.49	2.135
3	R^1=R^2=R^3=OCH_3; R^4=H	39.8	−4.56	2.166
4	R^1=OH; R^2=R^3=OCH_3; R^4=H	69.8	−6.14	2.071
5	R^1=OH; R^2=R^3=R^4=OCH_3	99.65	−4.56	1.655

*The IC_{50} of the derivatives against HepG2 cells was determined through MTT assay, as reported by Boonya-Udtayan *et al*. [1]

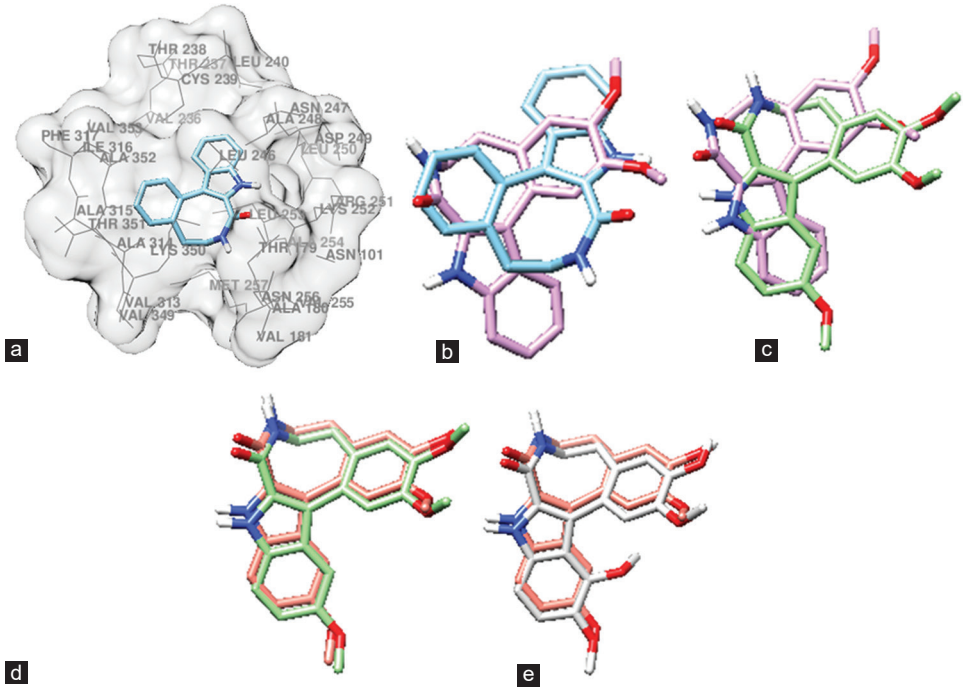

Fig. 3: Structural superpositions of indolobenzazocin-8-one derivatives in the tubulin colchicine-binding site, generated using UCSF Chimera [17]. Color-coded representations show: (a) Structure 1 (blue; unsubstituted reference conformation), (b) Structure 2 (pink) superimposed on Structure 1 (root-mean-square deviation [RMSD]=6.049 Å), (c) Structure 3 (green) superimposed on Structure 2 (RMSD=1.537 Å), (d) Structure 4 (orange) superimposed on Structure 3 (RMSD=0.483 Å), (e) Structure 5 (gray) superimposed on Structure 4 (RMSD=0.484 Å) RMSD values quantify backbone deviations of nitrogen atoms across all aligned structures

of the critical indole N–H···O=C(Lys350) hydrogen bond by 0.32 Å (Fig. 4c). These changes collectively raised the binding energy by 2.93 kcaL/moL (E_i=−4.56 kcaL/moL), indicating markedly reduced target engagement. The observed increase in $logD_{7.4}$ (2.166 vs. 2.135 in Structure 2) may be attributed to: (i) limited electron withdrawal from the single indole-positioned methoxy group, as oxygen's inductive effect is counterbalanced by its π-donor character, and (ii) enhanced molecular hydrophobicity due to resonance-driven electron delocalization into the aromatic system [28,29]. The net increase in lipophilicity ($\Delta logD_{7.4}$=+0.031) arises because the methoxy group's electron-donating resonance effects into the aromatic system outweigh its weaker electron-withdrawing inductive effects through the σ-bonded oxygen. The correlation between improved permeability indicators ($\Delta logD_{7.4}$=+0.031) and the 2.4-fold enhancement in potency (IC_{50}=39.8 μM vs. 96.23 μM in Structure 2) suggests that membrane permeation plays a dominant role in the anticancer activity of this structural series. This aligns with Lipinski's rule of five, where moderate lipophilicity ($logD_{7.4}$ 2.1–2.2) often optimizes cellular uptake while maintaining solubility.

Structure 4, featuring a hydroxyl substitution at R^1 in place of the methoxy group (cf. Structure 3), exhibited improved tubulin binding affinity (ΔE_i=−1.58 kcaL/moL; E_i=−6.14 kcaL/moL vs. −4.56 kcaL/moL). While the binding pose remained largely conserved (RMSD=0.483 Å; Fig. 3d) with identical hydrophobic interaction patterns (Fig. 4d), the -OH group introduced additional hydrogen bonding capacity through α-amino group and carbonyl oxygen of Asp249. This modification concurrently reduced lipophilicity ($logD_{7.4}$=2.071 vs. 2.166 in Structure 3), consistent with: (i) The hydroxyl group's higher hydrophilicity and (ii) its resonance electron withdrawal from the benzazocine ring. The observed inverse relationship between enhanced binding (lower E_i) and diminished cellular activity (higher IC_{50}) reinforces the dominant role of membrane permeability over target affinity in this structural series, mirroring trends observed in Structures 2–3 comparisons.

Structure 5, featuring an additional methoxy substitution at R^4 compared to Structure 4, exhibited reduced tubulin binding affinity (ΔE_i=+1.58 kcaL/moL; E_i=−4.56 kcaL/moL vs. −6.14 kcaL/moL). While the overall binding pose remained similar (RMSD=0.484 Å; Fig. 3e), the structural perturbation disrupted critical hydrogen bonding interactions mediated by the R^1 hydroxyl group (Fig. 4e). The 0.416 log unit reduction in lipophilicity ($logD_{7.4}$=1.655 for Structure 5 vs. 2.071 for Structure 4) mirrors the Structure 1→2 trend, where (i) dual adjacent methoxy groups on the indole-ring exhibit dominant inductive effects over resonance contributions and (ii) the substitution pattern forces the ring into a less planar geometry reducing hydrophobic surface area accessible for membrane partitioning [27].

Correlation analysis of molecular properties and cytotoxicity

Our Spearman's rank correlation analysis (selected for its robustness to non-normality and small sample size; n=5) revealed distinct relationships between molecular properties and cytotoxicity (IC_{50}).

(i) E_i versus IC_{50}: The scatter plot of E_i versus IC_{50} (Fig. 5a) revealed a moderate positive trend (ρ=0.46, p=0.434), though data dispersion was substantial. Notably, two compounds with similar E_i values (−4.56 kcal/moL) exhibited divergent IC_{50} values (39.8 vs. 99.65 μM), suggesting additional factors beyond binding energy influence potency.

(ii) $logD_{7.4}$ versus IC_{50}: In contrast, the $logD_{7.4}$-IC_{50} scatter plot (Fig. 5b) demonstrated a strong negative correlation (ρ=−0.90, p=0.037), with all data points adhering closely to the monotonic trend. The slope suggests a steep decrease in IC_{50} with increasing log $D_{7.4}$ within the studied range (1.66–2.26).

Advantages of indolobenzazocin-8-one over taxane drugs

Taxanes (e.g., paclitaxel, docetaxel) constitute a cornerstone class of anticancer agents, demonstrating clinical efficacy against diverse malignancies including breast, ovarian, and non-small cell lung cancers [30]. Their mechanism involves the stabilization of microtubule polymers, which paradoxically suppresses dynamic tubulin depolymerization/polymerization cycles required for mitotic spindle function [31,32]. This antimitotic action arrests proliferating cells in G2/M phase, ultimately triggering apoptosis [32]. Despite their

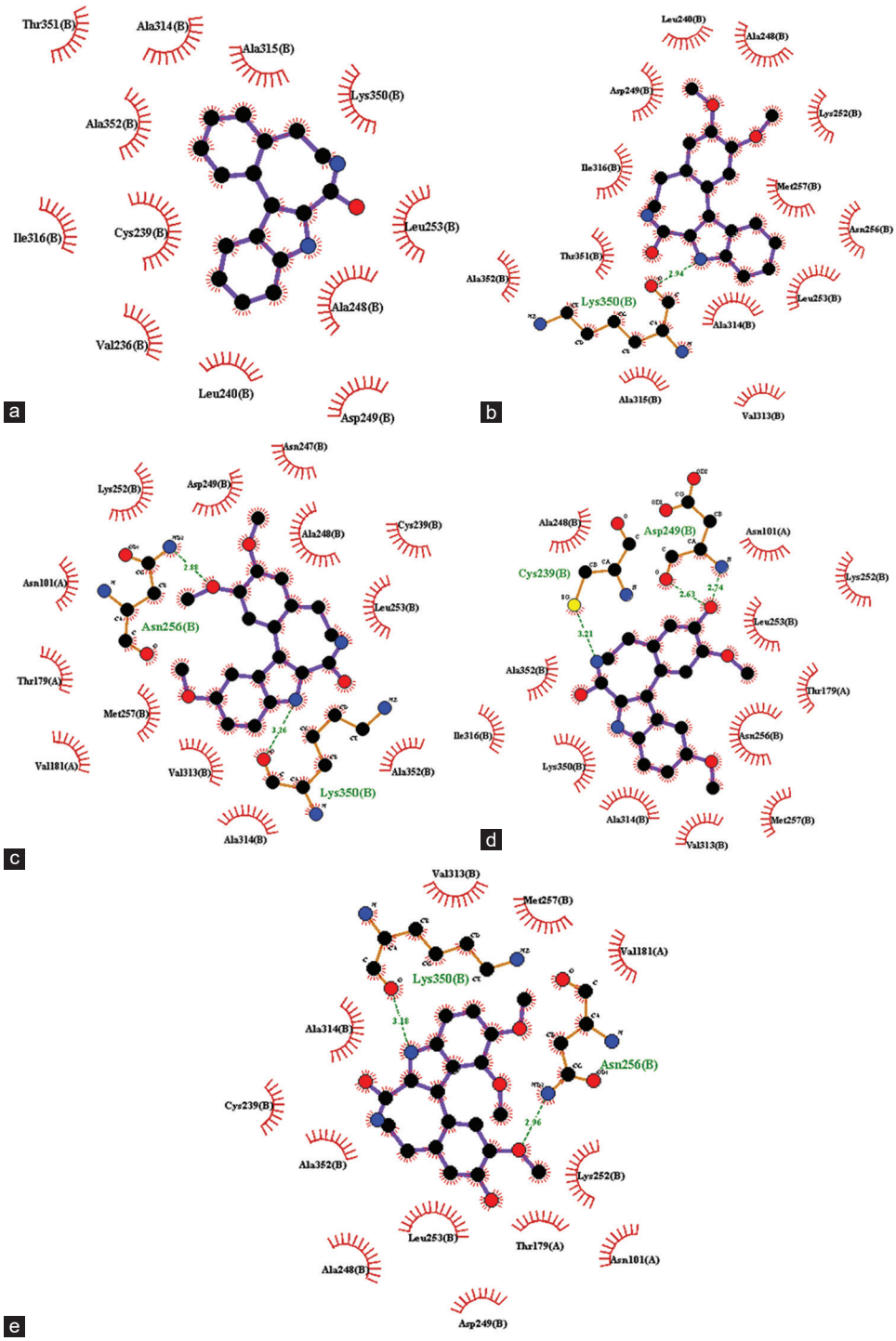

Fig. 4: Two-dimensional interaction diagrams of indolobenzazocin-8-one derivatives bound to the tubulin colchicine-binding site, generated using LigPlot+ [19]. Key interactions are shown for: (a) Structure 1: Unsubstituted core scaffold interactions, (b) Structure 2: R^1/R^2-dimethoxy derivative, (c) Structure 3: $R^1/R^2/R^3$-trimethoxy derivative, (d) Structure 4: R^1-hydroxy/R^2-methoxy derivative, (e) Structure 5: R^1-hydroxy/R^4-methoxy derivative

clinical efficacy, taxanes face significant pharmacological limitations due to inherently poor aqueous solubility, which complicates formulation and delivery [33,34]. These drugs also exhibit dose-limiting toxicities, including hepatotoxicity (elevated liver enzymes) and hematologic toxicity (neutropenia, anemia) [35]. Additional challenges arise from their susceptibility to P-glycoprotein-mediated efflux, which contributes to multidrug resistance [36], and the generation of genotoxic metabolites that raise safety concerns [37]. These factors are critical considerations in the evaluation of synthetic analogs and novel therapeutic compounds. They not only drive the rational design of new drug formulations but also inspire the development of structurally optimized derivatives to mitigate these adverse effects.

Table 2 summarizes the ADMETlab-predicted chemical and pharmacokinetic properties of indolobenzazocin-8-one (Structure 1). These indicators suggest potential advantages over the taxane class, including drug-like properties desirable for novel therapeutics.

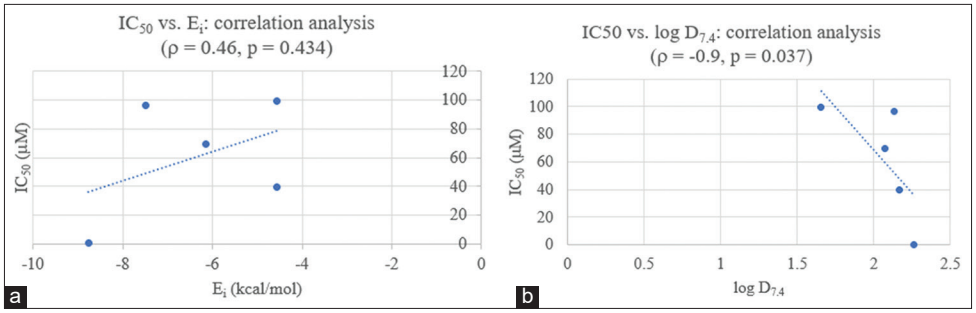

Fig. 5: Scatter plots of molecular properties versus cytotoxicity: (a) Ei versus IC_{50} (ρ=0.46, p=0.434), (b) IC50 versus log D7.4 (ρ=−0.9, p=0.037)

Table 2: Key drug-like properties of indolobenzazocin-8-one (Structure 1)

Property	Indicator	Optimum value*	Calculated value
Physicochemical (Lipinski's rule of five)	Molecular weight	≤500	262.11
	log D7.4 (log moL/L)	≤5	2.263
	Number of hydrogen bond acceptors	≤10	3.0
	Number of hydrogen bond donors	≤5	2.0
Absorption	Caco-2 permeability (log cm/s)	>−5.15	−5.033
	Probability of being p-gp inhibitor	-	0.859
	Probability of being p-gp substrate	-	0.117

*See complete explanation of all properties at https://admetmesh.scbdd.com/explanation/index

Evaluation results confirmed that indolobenzazocin-8-one (Structure 1) complies with Lipinski's rule of five, indicating favorable physicochemical properties and high predicted oral bioavailability. This suggests efficient absorption into the systemic circulation following oral administration. The compound also demonstrates favorable absorption characteristics, as evidenced by its high Caco-2 cell permeability. This *in vitro* measure of gastrointestinal tissue penetration further supports the physicochemical predictions, confirming indolobenzazocin-8-one's strong potential for effective gastrointestinal absorption.

The low probability of indolobenzazocin-8-one being a P-glycoprotein substrate (0.117), compared to its higher inhibitor probability (0.859) suggests minimal likelihood of P-gp-mediated efflux. This profile suggests that the compound more likely acts as a P-gp inhibitor rather than a substrate, potentially reducing efflux-mediated clearance and thereby enhancing systemic bioavailability.

These predictive indicators demonstrate that indolobenzazocin-8-one exhibits (i) favorable gastrointestinal absorption with minimal efflux, as supported by its Caco-2 permeability profile and Lipinski-compliant physicochemical properties and (ii) enhanced therapeutic potential through prolonged duration of action and reduced risk of P-gp-mediated cancer cell resistance – a key limitation of taxane therapies [38-40].

While these data highlight indolobenzazocin-8-one's potential advantages over taxanes, this should not be construed as suggesting an absence of therapeutic limitations. As with any novel compound, both efficacy and safety profiles require comprehensive evaluation through subsequent preclinical and clinical studies. While nearly all anticancer agents exhibit limitations, the current strategies such as targeted delivery systems and controlled-release formulations can help overcome these challenges [41-44]. However, such optimization approaches fall beyond the scope of the present study and will not be discussed here. The SAR of indolobenzazocin-8-one, particularly its demonstrated advantages over conventional taxane therapies, establishes a valuable foundation for (i) rational development of novel anticancer agents and (ii) optimization of drug formulations to enhance therapeutic efficacy. These structural insights provide critical data for future drug design initiatives.

Limitations

While our computational approach offers valuable structure-activity insights, certain limitations should be acknowledged. Docking predictions require experimental validation through *in vitro* assays or crystallography, and AutoDock4's rigid-receptor model may not account for tubulin flexibility. In addition, calculated log $D_{7.4}$ values may differ from experimental measurements. These constraints highlight important opportunities for future work without diminishing the observed trends.

CONCLUSION

This systematic SAR study reveals that the unsubstituted indolobenzazocin-8-one scaffold (Structure 1) achieves optimal anticancer activity (HepG2 IC_{50}=0.46 μM) by balancing two critical properties: (i) Strong tubulin binding affinity (E_i=−8.76 kcaL/moL) through conserved hydrogen bonding and hydrophobic interactions and (ii) enhanced cellular permeability (log$D_{7.4}$=2.263). -OCH_3 and –OH substitutions, while modulating electronic and steric properties, consistently compromised either target engagement (weaker tubulin binding by 1.27–4.20 kcaL/moL) or membrane penetration (reduced log$D_{7.4}$ by 0.128–0.608), leading to reduced potency (IC_{50} increased by 20–200 folds).

Computational ADMET profiling further highlights indolobenzazocin-8-one's drug-like advantages over taxanes: Lipinski compliance, high Caco-2 permeability (−5.033 log cm/s), and minimal P-gp efflux risk (probability=0.117). Its dual role as a tubulin binder and P-gp inhibitor (probability=0.859) may circumvent taxane resistance mechanisms while enabling oral administration. These findings provide a blueprint for future development: Preserving the core scaffold's geometry will be critical, while judicious substitutions may fine-tune pharmacokinetics without sacrificing potency. *In vivo* validation of this promising scaffold is warranted to assess its translational potential as a next-generation oral antimitotic agent.

ACKNOWLEDGMENT

We gratefully acknowledge the Department of Physical and Material Sciences, Faculty of Liberal Arts and Science, Kasetsart University (Kamphaeng-Saen Campus) for granting access to their facilities and for the provision of essential resources such as electricity, which were crucial for the completion of this work.

AUTHOR CONTRIBUTIONS

All authors have contributed to and approved the manuscript for publication.

CONFLICTS OF INTEREST

The authors state that there are no conflicts of interest regarding the publication of this paper.

FUNDING

The authors received no specific grant from any funding agency in the public, commercial, or not-for-profit sectors for the work reported herein.

REFERENCES

1. Boonya-Udtayan S, Eno M, Ruchirawat S, Mahidol C, Thasana N. Palladium-catalyzed intramolecular C-H amidation: Synthesis and biological activities of indolobenzazocin-8-ones. Tetrahedron. 2012;68(50):10293-10301. doi: 10.1016/j.tet.2012.10.011
2. Brancale A, Silvestri R. Indole, a core nucleus for potent inhibitors of tubulin polymerization. Med Res Rev. 2007;27(2):209-238. doi: 10.1002/med.20080, PMID 16788980
3. Colley HE, Muthana M, Danson SJ, Jackson LV, Brett ML, Harrison J, *et al*. An orally bioavailable, indole-3-glyoxylamide based series of tubulin polymerization inhibitors showing tumor growth inhibition in a mouse xenograft model of head and neck cancer. J Med Chem. 2015;58(23):9309-9333. doi: 10.1021/acs.jmedchem.5b01312, PMID 26580420
4. Kumbhar BV, Panda D, Kunwar A. Interaction of microtubule depolymerizing agent indanocine with different human αβ tubulin isotypes. PLoS One. 2018;13(3):e0194934. doi: 10.1371/journal.pone.0194934, PMID 29584771
5. Song J, Guan YF, Liu WB, Song CH, Tian XY, Zhu T, *et al*. Discovery of novel coumarin-indole derivatives as tubulin polymerization inhibitors with potent anti-gastric cancer activities. Eur J Med Chem. 2022;238:114467. doi: 10.1016/j.ejmech.2022.114467, PMID 35605363
6. Wittmann C, Dömötör O, Kuznetcova I, Spengler G, Reynisson J, Holder L, *et al*. Indolo[2,3-e]benzazocines and indolo[2,3-f]benzazonines and their copper(II) complexes as microtubule destabilizing agents. Dalton Trans. 2023;52(29):9964-9982. doi: 10.1039/d3dt01632c, PMID 37431840
7. Hong Y, Zhu YY, He Q, Gu SX. Indole derivatives as tubulin polymerization inhibitors for the development of promising anticancer agents. Bioorg Med Chem. 2022;55:116597. doi: 10.1016/j.bmc.2021.116597, PMID 34995858
8. Goel B, Jaiswal S, Jain SK. Indole derivatives targeting colchicine binding site as potential anticancer agents. Arch Pharm (Weinheim). 2023;356(10):e2300210. doi: 10.1002/ardp.202300210, PMID 37480173
9. Ren Y, Wang Y, Liu J, Liu T, Yuan L, Wu C, *et al*. X-ray crystal structure-guided discovery of novel indole analogues as colchicine-binding site tubulin inhibitors with immune-potentiating and antitumor effects against melanoma. J Med Chem. 2023;66(10):6697-6714. doi: 10.1021/acs.jmedchem.3c00011, PMID 37145846
10. Liu X, Jin J, Wu Y, Du B, Zhang L, Lu D, *et al*. Fluoroindole chalcone analogues targeting the colchicine binding site of tubulin for colorectal oncotherapy. Eur J Med Chem. 2023;257:115540. doi: 10.1016/j.ejmech.2023.115540, PMID 37301075
11. Hurysz B, Evans BA, Laryea RN, Boyer BE, Coburn TE, Dexter MS, *et al*. Synthesis, modeling, and biological evaluation of anti-tubulin indole-substituted furanones. Bioorg Med Chem Lett. 2023;90:129347. doi: 10.1016/j.bmcl.2023.129347, PMID 37236376
12. Li Y, Yang J, Niu L, Hu D, Li H, Chen L, *et al*. Structural insights into the design of indole derivatives as tubulin polymerization inhibitors. FEBS Lett. 2020;594(1):199-204. doi: 10.1002/1873-3468.13566, PMID 31369682
13. Xia LY, Zhang YL, Yang R, Wang ZC, Lu YD, Wang BZ, *et al*. Tubulin inhibitors binding to colchicine-site: A review from 2015 to 2019. Curr Med Chem. 2020;27(40):6787-67814. doi: 10.2174/0929867326666191003154051, PMID 31580244
14. Li W, Shuai W, Sun H, Xu F, Bi Y, Xu J, *et al*. Design, synthesis and biological evaluation of quinoline-indole derivatives as anti-tubulin agents targeting the colchicine binding site. Eur J Med Chem. 2019;163:428-442. doi: 10.1016/j.ejmech.2018.11.070, PMID 30530194
15. Li W, Sun H, Xu F, Shuai W, Liu J, Xu S, *et al*. Synthesis, molecular properties prediction and biological evaluation of indole-vinyl sulfone derivatives as novel tubulin polymerization inhibitors targeting the colchicine binding site. Bioorg Chem. 2019;85:49-59. doi: 10.1016/j.bioorg.2018.12.015, PMID 30599412
16. Hanwell MD, Curtis DE, Lonie DC, Vandermeersch T, Zurek E, Hutchison GR. Avogadro: An advanced semantic chemical editor, visualization, and analysis platform. J Cheminform. 2012;4(1):17. doi: 10.1186/1758-2946-4-17, PMID 22889332
17. Pettersen EF, Goddard TD, Huang CC, Couch GS, Greenblatt DM, Meng EC, *et al.* UCSF Chimera--a visualization system for exploratory research and analysis. J Comput Chem. 2004;25(13):1605-1612. doi: 10.1002/jcc.20084, PMID 15264254
18. Morris GM, Huey R, Lindstrom W, Sanner MF, Belew RK, Goodsell DS, *et al*. Autodock4 and autodocktools4: Automated docking with selective receptor flexibility. J Comput Chem. 2009;30(16):2785-2791. doi: 10.1002/jcc.21256, PMID 19399780
19. Laskowski RA, Swindells MB. LigPlot+: Multiple ligand-protein interaction diagrams for drug discovery. J Chem Inf Model. 2011;51(10):2778-2786. doi: 10.1021/ci200227u, PMID 21919503
20. Corporation M, Microsoft. Excel. Microsoft 365, Microsoft 2024.
21. O'Boyle NM, Banck M, James CA, Morley C, Vandermeersch T, Hutchison GR. Open babel: An open chemical toolbox. J Cheminform. 2011;3(1):33. doi: 10.1186/1758-2946-3-33, PMID 21982300
22. Fu L, Shi S, Yi J, Wang N, He Y, Wu Z, *et al*. ADMETlab 3.0: An updated comprehensive online ADMET prediction platform enhanced with broader coverage, improved performance, API functionality and decision support. Nucleic Acids Res. 2024;52(W1):W422-W431. doi: 10.1093/nar/gkae236, PMID 38572755
23. ACD. Version 14.01. Chem, Sketch (Freeware), Toronto, ON, Canada: Advanced Chemistry Development, Inc.; 2015. Available from: https://www.acdlabs.com
24. Kotthoff I, Kundrotas PJ, Vakser IA. Dockground scoring benchmarks for protein docking. Proteins. 2022;90(6):1259-1266. doi: 10.1002/prot.26306, PMID 35072956
25. Bocianowski J, Wrońska-Pilarek D, KrysztofiakKaniewska A, Matusiak K, Wiatrowska B. Comparison of Pearson's and spearman's correlation coefficients for selected traits of *Pinus sylvestris* L. Biom Lett. 2024;61(2):115-135.
26. Eclarin PR, Yan PA, Paliza CL, Ibasan B, Basiloy PR, Gante NA, *et al*. Benchmarking the distribution coefficient of anticancer lead compounds using the predicted log D values of clinically approved chemotherapeutic drugs. J Prev Diagn Treat Strateg Med. 2022;1(2):143-152. doi: 10.4103/jpdtsm.jpdtsm-31-22
27. Veber DF, Johnson SR, Cheng HY, Smith BR, Ward KW, Kopple KD. Molecular properties that influence the oral bioavailability of drug candidates. J Med Chem. 2002;45(12):2615-2623. doi: 10.1021/jm020017n, PMID 12036371
28. Zavrsnik D, Spirtović S, Muratović S. The 4-arylaminocoumarin derivatives log P values calculated according to Rekker's method. Bosn J Basic Med Sci. 2003;3(4):37-40. doi: 10.17305/bjbms.2003.3491, PMID 16232136
29. Keruckas J, Lygaitis R, Simokaitiene J, Grazulevicius JV, Jankauskas V, Sini G. Influence of methoxy groups on the properties of 1,1-bis(4-aminophenyl)cyclohexane based arylamines: Experimental and theoretical approach. J Mater Chem. 2012;22(7):3015-3027. doi: 10.1039/c2jm14387a
30. Sparano JA, Gray RJ, Ravdin PM, Makower DF, Pritchard KI, Albain KS, *et al*. Clinical and genomic risk to guide the use of adjuvant therapy for breast cancer. N Engl J Med. 2019;380(25):2395-2405. doi: 10.1056/NEJMoa1904819, PMID 31157962
31. Dumontet C, Jordan MA. Microtubule-binding agents: A dynamic field of cancer therapeutics. Nat Rev Drug Discov. 2010;9(10):790-803. doi: 10.1038/nrd3253, PMID 20885410
32. Schiff PB, Fant J, Horwitz SB. Promotion of microtubule assembly *in vitro* by Taxol. Nature. 1979;277(5698):665-667. doi: 10.1038/277665a0, PMID 423966
33. Škubník J, Pavlíčková V, Ruml T, Rimpelová S. Current perspectives on taxanes: Focus on their bioactivity, delivery and combination therapy. Plants (Basel). 2021;10(3):569. doi: 10.3390/plants10030569, PMID 33802861
34. Lei L, Wang XJ, Tang SC. Novel taxanes in development: Hopes or hypes? Crit Rev Oncol Hematol. 2022;176:103727. doi: 10.1016/j.critrevonc.2022.103727, PMID 35644326
35. Jabir RS, Naidu R, Annuar MA, Ho GF, Munisamy M, Stanslas J. Pharmacogenetics of taxanes: Impact of gene polymorphisms of drug transporters on pharmacokinetics and toxicity. Pharmacogenomics. 2012;13(16):1979-1988. doi: 10.2217/pgs.12.165, PMID 23215890
36. Brooks TA, Kennedy DR, Gruol DJ, Ojima I, Baer MR, Bernacki RJ. Structure-activity analysis of taxane-based broad-spectrum multidrug

resistance modulators. Anticancer Res. 2004;24(2A):409-415. PMID 15152938

37. Wang Y, Feng F, Chen L, Zhao H, Tian L. Isolation, identification and characterization of potential impurities in cabazitaxel and their formation. Magn Reson Chem. 2014;52(12):783-788. doi: 10.1002/mrc.4125, PMID 25123687
38. Tian Y, Lei Y, Wang Y, Lai J, Wang J, Xia F. Mechanism of multidrug resistance to chemotherapy mediated by P-glycoprotein (Review). Int J Oncol. 2023;63(5):119. doi: 10.3892/ijo.2023.5567, PMID 37654171
39. Alalawy AI. Key genes and molecular mechanisms related to paclitaxel resistance. Cancer Cell Int. 2024;24(1):244. doi: 10.1186/s12935-024-03415-0, PMID 39003454
40. Al-Thubiani WS. The role of P-glycoprotein (P-GP) in cancer multidrug resistance (MDR): Challenges for inhibiting P-GP in the context of overcoming MDR. J Pharm Res Int. 2023;35(23):44-58. doi: 10.9734/jpri/2023/v35i237422
41. A. M. H.V., Namboori PKK. Design and development of a pharmacogenomic model for breast cancer to study the variation in drug action and side effects. Int J Appl Pharm. 2022;14(3):61-68.
42. Dwipoyono B, Choirunisa S, Nadjib M, Sjaaf AC. Cost analysis of taxane-based and cisplatin-based chemotherapy regimens for epithelial ovarian cancer in Dharmais national cancer hospital. Int J Appl Pharm. 2017;9:172-175.
43. Handayani F, Fitria N, Sari YO, AA. Impact of the combination of doxorubicin, cyclophosphamide, and docetaxel on CA 15-3 biomarker levels in breast cancer patients: A comparative study between delayed and non-delayed chemotherapy. Int J Appl Pharm. 2025;17(1):82-88. doi: 10.22159/ijap.2025.v17s1.12
44. Hemant K, Raizaday A, Sivadasu P, Uniyal S, Hemanth Kumar S. Cancer nanotechnology: Nanoparticulate drug delivery for the treatement of cancer. Int J Pharm Pharm Sci. 2015;7(3):40-46.